Solar Energy Materials and Solar Cells 173 (2017) 85–91

Contents lists available at ScienceDirect

Solar Energy Materials and Solar Cells

journal homepage: www.elsevier.com/locate/solmat

Improvement of the SRH bulk lifetime upon formation of n-type POLO junctions for 25% efficient Si solar cells

Jan Krügener[a,*], Felix Haase[b], Michael Rienäcker[b], Rolf Brendel[b,c], H.Jörg Osten[a,c], Robby Peibst[a,b]

[a] Institute of Electronic Materials and Devices (MBE), Leibniz Universität Hannover, Schneiderberg 32, 30167 Hannover, Germany
[b] Institute for Solar Energy Research Hamelin (ISFH), Am Ohrberg 1, 31860 Emmerthal, Germany
[c] Laboratory of Nano and Quantum Engineering (LNQE), Leibniz Universität Hannover, Schneiderberg 39, 30167 Hannover, Germany

ARTICLE INFO

Keywords:
Passivating contact
Polysilicon
Gettering
Silicon solar cell

ABSTRACT

Carrier-selective contact schemes, like polysilicon on oxide (POLO), provide low contact resistivities while preserving an excellent passivation quality. These junctions offer an important additional feature compared to a-Si/c-Si heterojunctions. We find that the formation of *n*-type POLO junctions lead to a huge increase of the Shockley-Read-Hall (SRH) lifetime of the substrate, a prerequisite for highly efficient solar cells. The SRH lifetime improvement can be observed for both bulk polarities and for a variety of bulk resistivities. Thus we suggest that the highly doped POLO junction getters impurities that have more or less symmetric SRH capture cross sections. We are able to achieve SRH lifetimes of > 50 ms. By applying POLO junctions to interdigitated back contact cells, we achieve cells with an efficiency of 25%.

1. Introduction

Passivating contacts in combination with the interdigitated back contact (IBC) cell design enable the so far highest energy conversion efficiencies of up to 26.6% for single junction silicon solar cells [1]. Currently, two types of passivating contacts are used for IBC cells: a-Si/c-Si heterojunctions and polycrystalline on oxide (POLO) junctions [2,3].

POLO junctions, as used in this work, exhibit high temperature stability which might be beneficial for industrialization applying conventional high temperature process techniques. Furthermore we find that even for high quality FZ wafers the Shockley-Read-Hall (SRH) limitation of bulk lifetime can be significantly reduced during the high-temperature *n*-type POLO junction formation step. We systematically study this aspect on different bulk polarities and resistivities. Finally we use these results to prepare IBC solar cells with an independently confirmed efficiency of 25% and an efficiency potential exceeding 26%.

2. Experimental

We use *n*-type and *p*-type FZ wafers with resistivities between 1.5 Ωcm and 90 Ωcm. The samples are either passivated with Al_2O_3 or with POLO junctions. The latter are prepared as follows. After thermal oxidation (~ 2.2 nm), 225 nm intrinsic polysilicon (poly-Si) is deposited by low pressure chemical vapour deposition. The poly-Si is *ex situ* doped by ion implantation, either with boron ($N_A \approx 1 \times 10^{20}$ cm^{-3}), phosphorus ($N_D \approx 2 \times 10^{20}$ cm^{-3}), or both (*n*-type counter-doped ($N_D \approx 1 \times 10^{20}$ cm^{-3}) [4]). After junction formation (990–1080 °C), all samples are characterized by photoconductance decay method (PCD). Emitter saturation current densities (J_{0e}) are extracted by applying the method of Kane & Swanson [5]. The measured effective lifetimes were decomposed into limitations implied by the surface (using the J_{0e} values), by Auger and radiative recombination (using the model of Richter et al. [6]), and by the SRH recombination within the substrates. The lifetime of the surface recombination (τ_{surf}) is calculated by using following equation: $\tau_{surf} = (q \times n_i^2 \times W)/([\Delta n + n_0 + p_0] \times J_{0e})$. With q the elementary charge, n_i the intrinsic charge carrier density, W the substrate width, Δn the excess carrier density and n_0/p_0 the equilibrium chare carrier densities. An injection-independent SRH lifetime (τ_{SRH}) was used as a fitting parameter in order to reproduce the measured effective lifetimes. Any injection dependency of τ_{SRH} would lead to an unreasonable amount of fit parameters (capture cross sections, energetic position of the trap level, etc.), possibly causing unreliable results. From this simplification, the relative uncertainty of the extracted lifetimes represents the uncertainty of the measurement itself, which is around 20% [6]. Fig. 1 shows an exemplary comparison of τ_{SRH} determination using the intercept method of Kane & Swanson (Fig. 1a) and the above described fitting procedure of the measured trend of τ_{eff}

* Corresponding author.
E-mail address: kruegener@mbe.uni-hannover.de (J. Krügener).

http://dx.doi.org/10.1016/j.solmat.2017.05.055
Received 6 April 2017; Received in revised form 22 May 2017; Accepted 23 May 2017
Available online 31 May 2017

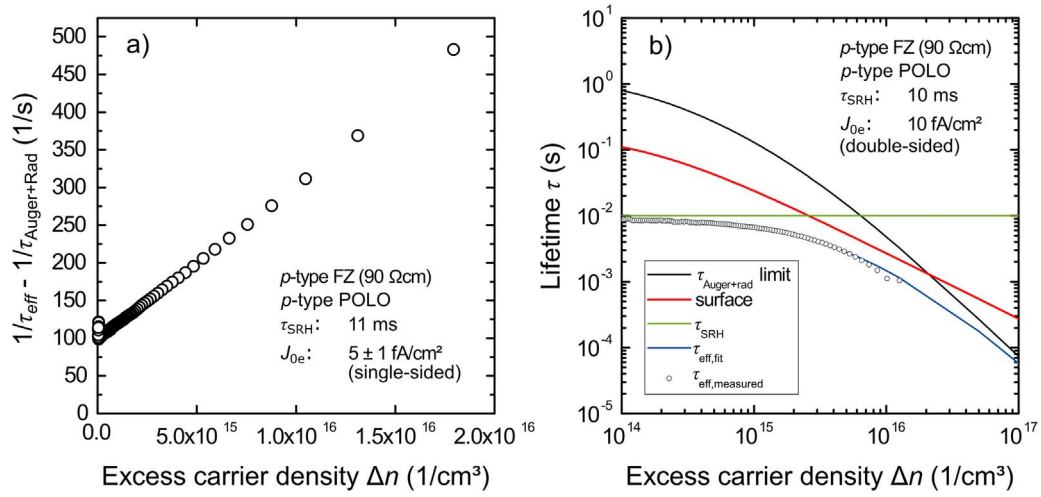

Fig. 1. a) inverse minority carrier lifetime, corrected for Auger and radiative recombination [6] and b) measured lifetime and its single components as a function of the excess carrier density of a *p*-type POLO junction on *p*-type FZ substrate (90 Ωcm). The junction is formed at 1050 °C.

as a function of the excess carrier density (Fig. 1b). Both methods are in good agreement, although τ_{SRH} after Kane & Swanson tends to give slightly higher τ_{SRH} values (11 ms instead of 10 ms in this case). This trend is also observed in multiple lifetime analysis on various other samples (not shown here).

Based on the observation of an improvement of τ_{SRH} upon gettering in *n*-type POLO junctions, we include this step into the fabrication process for interdigitated back contact solar cells [3].

3. Results and discussion

3.1. Improvement of the SRH lifetime upon junction formation

The impact of the POLO junction formation is found to be very similar for all substrate polarities and resistivities. Therefore the results will exemplary be discussed by means of the 90 Ωcm *p*-type substrates. Here we first focus on samples annealed at 1050 °C since this is around the optimum for the used interfacial oxide [7]. In Fig. 2, the measured effective lifetimes are plotted as a function of the excess carrier density after POLO junction formation. Furthermore, the modelled contributions from the surfaces, the bulk (τ_{SRH}) as well as Auger and radiative recombination are also shown. Around the implied maximum power point (MPP, $\Delta n \approx 2 \times 10^{15}\,cm^{-3}$) the effective lifetime in the sample with *p*-type POLO junctions is limited by a comparatively low τ_{SRH} value of 11 ms (Fig. 2a). This is different for the samples with *n*-type POLO junctions (Fig. 2b & c). Here much higher τ_{SRH} values of 50 ms are obtained. These modelled values of τ_{SRH} can only be considered as lower limits since even higher values of τ_{SRH} do not impact the effective lifetime characteristic anymore.

Additionally the corresponding implied *J-V* curves are given in Fig. 3. Compared to Fig. 2 some extra information can be recognized. For the *p*-type POLO junctions the slope of the curve significantly changes across the displayed voltage range (Fig. 3a) which is not the case for the *n*-type POLO junctions (Fig. 3b & c). This behavior is mirrored in the extracted ideality factors at the MPP of 1.27 for *p*-type POLO, 1.00 for *n*-type POLO and 1.03 for counter-doped *n*-type POLO junctions. This strong decrease in ideality factor around MPP comes in hand with an increases implied fill factor (*ipFF*) after *n*-type POLO junction formation. Here an *ipFF* of 84.4% for *p*-type POLO and up to 86.2% for *n*-type POLO junctions is extracted. Our hypothesis for this improvement is a very effective external gettering of recombination-active impurities by the *n*-type POLO layers. The corresponding effects and mechanisms are discussed in the following sections.

Fig. 4 summarizes the extracted τ_{SRH} values for all investigated base resistivities and polarities. After cleaning and surface passivation with Al_2O_3 (but apart from that "out-of-box"), the *p*-type wafers have SRH lifetimes around 14 ms except for the 3.7 Ωcm material (~ 1 ms). The *n*-type substrates feature SRH lifetimes of 4 ms and 10 ms after Al_2O_3

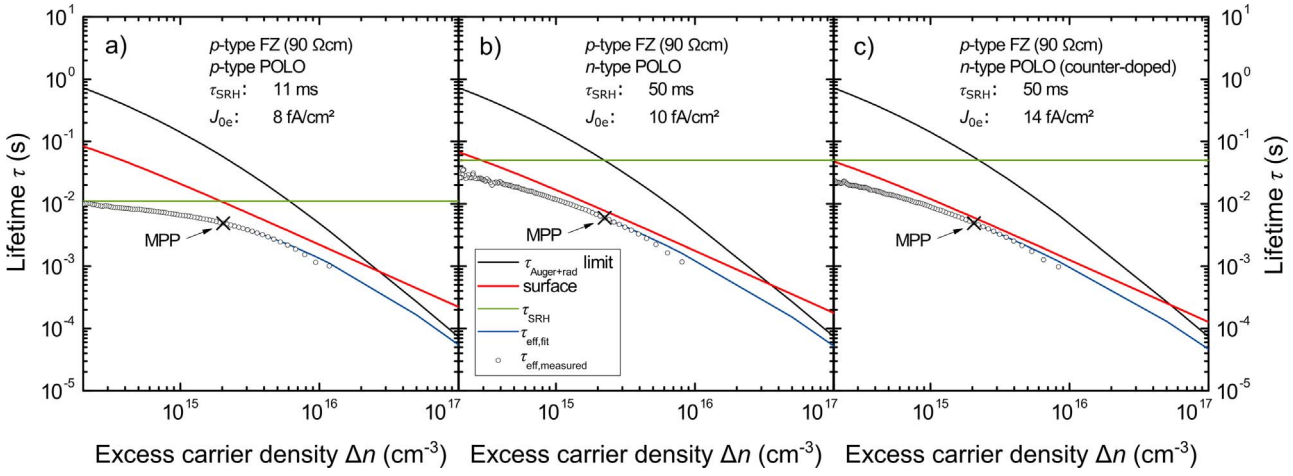

Fig. 2. Measured effective carrier lifetimes as a function of the excess carrier density on *p*-type substrates. a) *p*-type POLO, b) *n*-type POLO and c) *n*-type counter-doped POLO junctions. The modelled charge carrier lifetimes for Auger and radiative, SRH and surface recombination are also shown. J_{0e} accounts for the total value of a double-sided sample. All samples are annealed at 1050 °C.

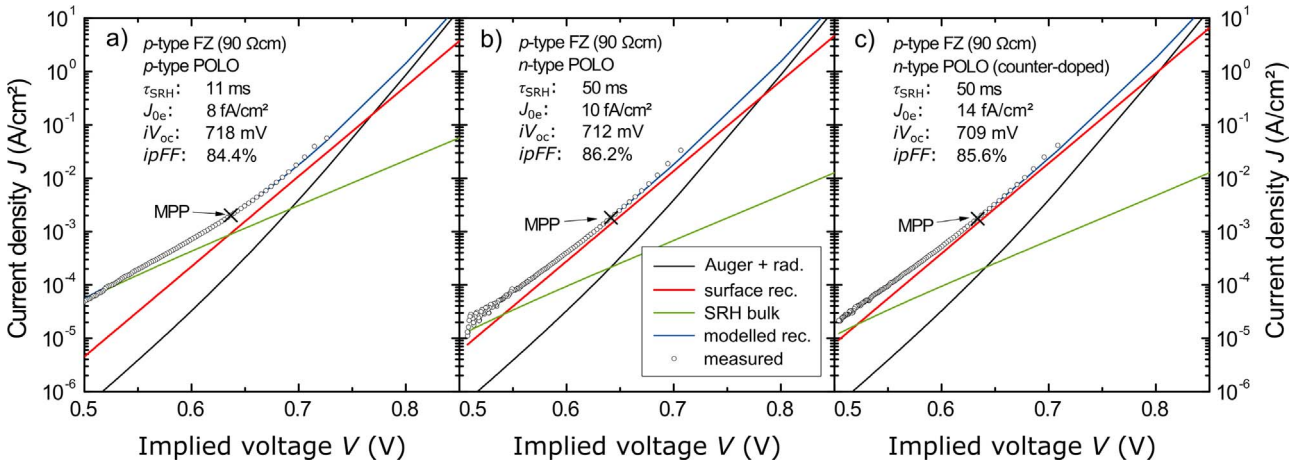

Fig. 3. Implied *J-V* curves corresponding to the measured lifetimes as a function of the excess carrier density from Fig. 2. Additionally the implied open circuit voltage iV_{oc} and the implied pseudo fill factor *ipFF* are given, assuming a generation current density of 42 mA/cm^2.

passivation. The formation of *p*-type POLO junctions apparently leads to differences in τ_{SRH} depending on the bulk polarity. On *p*-type substrates, the formation of *p*-type POLO junctions seems to result in a significant decrease of τ_{SRH}. On *n*-type substrates no difference between the Al_2O_3-passivated references and the *p*-type POLO-passivated samples can be observed. We find in infrared lifetime measurements (ILM [8], not shown here) that the lifetime in the center of the samples with *p*-type POLO on *p*-type substrates is not homogeneously distributed. Some, very localized, spots with a highly reduced lifetime exist which are imbedded by regions with lifetimes as high as for the reference samples. Thus the lifetimes extracted from PCD can be considered as averaged values in the samples center. This mentioned inhomogeneity cannot be observed on the *n*-type substrates, where the reference samples and the *p*-type POLO ones show more or less the same τ_{SRH} (see Fig. 4b). The origin of this difference is not clearly understood so far and needs further investigation.

On the other hand, upon formation of *n*-type POLO junctions (independent if phosphorus-doped or counter-doped), τ_{SRH} is increased above 100 ms. For such high τ_{SRH} the recombination at the surfaces dominates the overall recombination around the MPP (see crosses in Figs. 2 and 3). Since a further increase of τ_{SRH} to even higher values has no effect on the modelled effective lifetimes, the specified τ_{SRH} values for *n*-type POLO junctions pose lower limits (indicated by open symbols in Fig. 4). In some cases (lower base resistivity), the τ_{SRH} values are even higher than the lifetimes limited by Auger and radiative recombination. In these cases the bulk lifetime is dominated by Auger recombination. Especially for the lower resistivity samples the uncertainty of the extracted τ_{SRH} is very high due to the uncertainties of the measurement as well as of the used models. A detailed analysis of the uncertainty is subject of further work.

The effect of increasing τ_{SRH} after *n*-type POLO junction formation is especially pronounced for lower quality base materials. In our case the 3.7 Ωcm *p*-type substrates have a low initial τ_{SRH} of around 1 ms. After *n*-type junction formation, τ_{SRH} increases up to 50 ms for the phosphorus-doped and even up to 100 ms for the counter-doped samples.

We are currently systematically evaluating whether this lifetime improvement upon *n*-type POLO junction formation can also be achieved on industrially relevant Czochralski-grown (Cz) substrates. First attempts using *n*-type POLO junctions on 4.4 Ωcm *n*-type Cz substrates (thickness of interfacial oxide ~ 2.4 nm) show that as high SRH lifetimes as 100 ms can be obtained after junction formation below 1000 °C. This is consistent to previous findings of Römer et al. [4]. More detailed investigations are under work to further quantify the lifetime improvement for Cz or even for multicrystalline wafers.

3.2. Impact of the annealing conditions

For the used interfacial oxide (~ 2.2 nm) the optimum annealing temperature (i.e. for the lowest J_{0e}) is around 1050 °C, e.g. [7]. Lower temperatures potentially lead to an insufficient break-up of the oxide and thus to an increased series resistance in a final solar cell. Too high annealing temperatures can completely destroy the oxide layer and therefore degrade the passivation quality of the junction. The impact of the annealing temperature on SRH lifetimes of POLO junctions has not

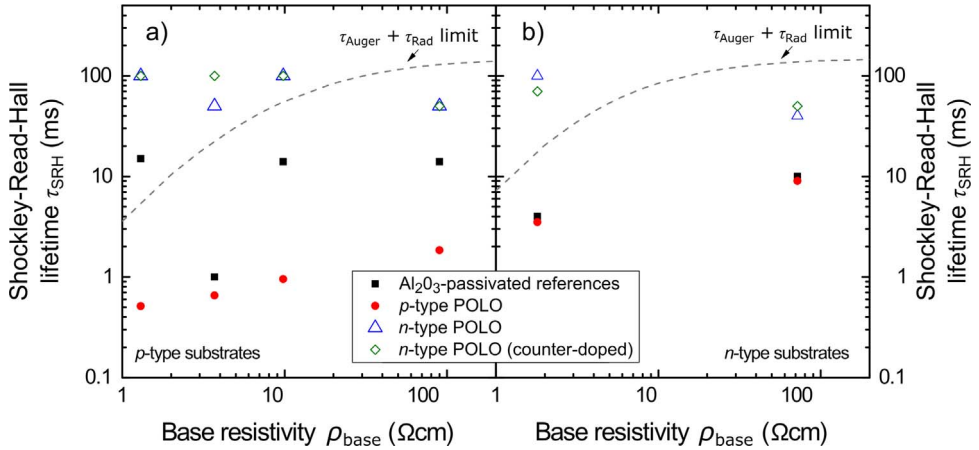

Fig. 4. Calculated τ_{SRH} for different POLO junctions and Al_2O_3-passivated references on a) *p*-type and b) *n*-type FZ substrates as a function of the base resistivity. Open symbols correspond to a lower lifetime limit. The combined limits of Auger and radiative recombination [6] are also shown as broken lines.

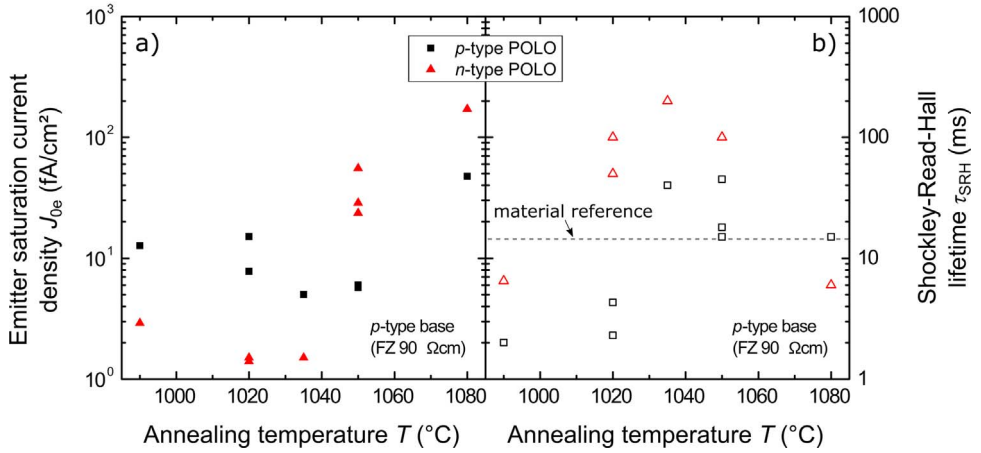

Fig. 5. a) Measured J_{0e} for different annealing temperatures for *p*-type and *n*-type POLO junctions and b) corresponding modelled τ_{SRH}.

been studied so far. In order to understand the mechanisms behind the improvement of the SRH lifetime after junction formation we vary the junction formation temperature around this optimum (990 °C – 1080 °C). Within this temperature range, no thermally activated defects related to the FZ substrates are expected [9].

Fig. 5 shows the measured J_{0e} values after junction formation as well as the corresponding modelled τ_{SRH}. First we will discuss the behavior of the *p*-type POLO junctions. The emitter saturation current density J_{0e} decreases for increasing annealing temperatures up to 1035 °C. Around this optimum J_{0e} values as low as 5 fA/cm^2 are observed and even lower ones for *n*-type POLO (see below). At 1080 °C J_{0e} increases up to 47 fA/cm^2. The modelled SRH lifetime shows a corresponding trend with a maximum τ_{SRH} after annealing between 1035 °C and 1050 °C. Around this optimum τ_{SRH} varies between 15 ms and 50 ms whereas the lifetime is homogeneously distributed within the sampled region as checked by ILM (not shown here).

The *n*-type POLO junctions show very low J_{0e} values (down to 1.4 fA/cm^2) for annealing temperatures below 1050 °C. The low J_{0e} values are accompanied by very high SRH lifetimes above 100 ms (see Fig. 5b). Again these values can be considered as lower limits since a further increase does not impact the resulting τ_{eff} vs. Δn plot anymore. In contrast to the *p*-type junctions, τ_{SRH} is improved (~ 100 ms) even for comparably high J_{0e} above 20 fA/cm^2 after annealing at 1050 °C. However, for the lowest and the highest annealing temperatures investigated (990 °C and 1080 °C, respectively) we do not observe an improvement of τ_{SRH} upon *n*-type POLO junction formation. We tentatively conclude that the structure of the interfacial oxide – either continuously intact, locally perforated at some spot or perforated in larger areas – influences the efficiency of the lifetime improvement.

3.3. Possible origin(s) of the lifetime improvement

By now the process sequences for low emitter saturation current densities and low contact resistivity values of POLO junctions are known quite well [4,10]. Nevertheless, the mechanisms behind the improvement of SRH lifetime after POLO junction formation are not completely understood yet. Furthermore the specific impurity limiting the SRH lifetime before gettering and its origin are unknown so far. In literature several gettering mechanisms are discussed [11]. In the following we give an overview of those mechanisms which might be involved in SRH lifetime enhancement during POLO junction formation. Afterwards we try to identify the gettered species.

In microelectronic industry gettering of metal impurities by back side deposition of polysilicon and subsequent annealing is a well-known technique [11,12]. In this case two mechanisms are discussed: segregation gettering (SG) and relaxation gettering (RG). SG is driven by different temperature-dependent equilibrium concentrations within poly-Si and c-Si (higher in poly-Si e.g. [12] for iron). RG is caused by a local supersaturation of the impurities during cooling and strongly depends on the cooling rate [12].

The diffusivity *D* of most transition metals is several orders of magnitude lower in silicon dioxide compared to silicon [13–15]. For example for iron at 1050 °C, D_{Si} is 2.7 × 10^{-6} cm^2/s [14] whereas D_{SiO2} is only around 4.2 × 10^{-14} cm^2/s [15]. Since the impurity has to diffuse fast into the phase with the higher solubility, RG can be neglected for our samples [12]. A positive effect caused by the presence of pinholes (i.e. regions of direct contact between c-Si and poly-Si) within the oxide is possible, although the pinhole areal density is small [16,17].

Gettering of the poly-Si caused by a different solubility of transition metals within poly-Si and c-Si should be more or less identical for both POLO junction polarities (neglecting any impact of the dopant species and its concentration on the crystalline structure of the poly-Si). The results in Section 3.2 show that under ideal conditions an improvement of τ_{SRH} can be achieved using any dopant polarity. However, the process window for *n*-type POLO junctions is wider and the absolute values of τ_{SRH} which can be obtained are much higher compared to *p*-type POLO. Therefore gettering by a higher solubility in the poly-Si cannot be the only mechanism behind the improvement.

Another effect which might contribute to the gettering could be connected with high dopant concentrations. The highly-doped regions can increase the local solubility of metals due to the position of the Fermi level [11]. Furthermore, ionized dopant atoms can attract charged metal atoms and form metal-dopant pairs, e.g. Fe-B pairs [18]. Applied to the samples presented here, two regions of the POLO junction can contribute to this effect: the highly-doped poly-Si and an in-diffused region right underneath the interfacial oxide. The in-diffusion is formed during junction formation by diffusion of dopants through the interfacial oxide into the substrate [4,19]. Furthermore a solubility enhancement by Fermi level effects, an increase of the substitutional fraction of metals, and a gettering to SiP particles (similar to what can be observed in $POCl_3$ diffusions [18]) might occur. These effects might be very efficient due to high P concentration in the poly-Si (> 10^{20} cm^{-3}).

From our results we can deduce several characteristic properties of the gettered impurity. First it must affect both bulk polarities (deep level, more or less symmetric capture cross sections). Otherwise the difference between references and gettered samples would be much less for one or the other polarity. Next, the capture cross sections and/or the initial impurity concentration has to be quiet low. If not the lifetimes of the reference samples are expected to be much lower. At last the wanted impurity has to be gettered better by *n*-type than by *p*-type POLO.

Typical impurity species in silicon are iron, chromium, copper,

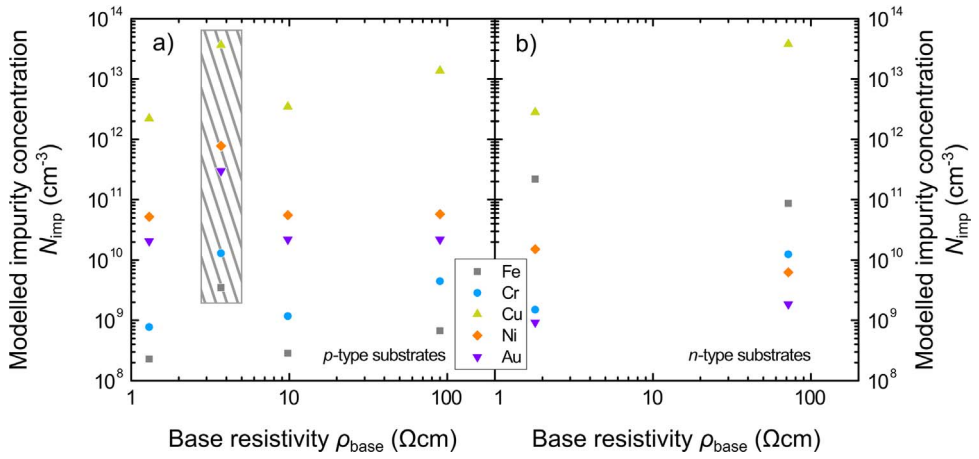

Fig. 6. Modelled impurity densities as a function of the bulk resistivity for a) *p*-type and b) *n*-type substrates. Recombination parameters are taken from [20,21].

nickel and gold. Iron, copper and gold show very asymmetric carrier capture cross sections [20,21] and are therefore most unlikely the wanted species. Furthermore Fe and Cu are known to be easily gettered by high boron concentrations [22,23] whereas Ni is not [23]. On the other hand Ni can be gettered by $POCl_3$ diffusion [24,25]; same for Au [26] and Cr [27]. Thus Cr or Ni might possibly be the wanted impurity.

On this account we model the SRH lifetime for all reference samples in Section 3.1 for Fe, Cr, Cu, Ni and Au using the Shockley-Read-Hall equation [28,29]. The corresponding capture cross sections and energy levels are taken from [20] and the reference therein for Fe, Cr, Cu and Ni. For Au the values from [21] are used. To mirror the SRH lifetime extracted from the PCD measurements we use the density of the impurity (N_{imp}) as the fit parameter.

The resulting modelled impurity densities as a function of the bulk resistivity are summarizes in Fig. 6 (assuming only one of the species present in each case). Due to its low initial lifetime, the 3.7 Ωcm *p*-type substrates break ranks whereas these samples will be excluded from the following considerations (highlighted with a grey background). Aside from that some characteristics can be deduced from these results. On *p*-type substrates (Fig. 6a) the concentrations of Fe, Cr and Cu need to be increased for increasing base resistivity to mirror the corresponding τ_{SRH}. For Au and Ni nearly constant concentrations around 2×10^{10} cm^{-2} and 5×10^{10} cm^{-2}, respectively, can be found. For *n*-type substrates no dependency can be observed (Fig. 6b). Thus identifying one especially recombination active species responsible for the lifetime limitation is not possible.

From all of these considerations a few distinct conclusions can be drawn. First, SRH lifetime improvement is much more effective for *n*-type than for *p*-type POLO junction formation. The maximum improvement comes along with very low emitter saturation current densities. The high observed SRH lifetimes after *n*-type POLO formation indicate that aside from poly-Si gettering a component caused by high phosphorus concentrations might support the overall gettering. The wanted defect species could be Ni or a Ni-like species based on the above stated characteristics: harms both polarities, gettered only by high concentrations of P and furthermore the modelled concentration is nearly constant for all *p*-type and *n*-type samples, respectively. Nevertheless, all of the mentioned mechanism and effects might contribute to the SRH lifetime improvement after junction formation and we cannot determine the dominating mechanisms from our experiment. Somewhat surprising is that there are obviously contaminations present in all investigated commercially available floatzone wafers. One possible origin of these contaminations might be the wafer sawing process as found for multicrystalline wafers [30]. A more detailed investigation of these details is subject of further work.

3.4. Solar cell results

For high efficiency solar cells a very high τ_{SRH} is essential [31]. On this account, we intentionally introduce an additional *n*-type POLO junction on the front side in the process flow of our *p*-type (1.5 Ωcm) interdigitated back contact (IBC) solar cells (Fig. 7). This junction is present during junction formation and is removed during front-side texturing to avoid parasitic absorption and to improve light trapping (Fig. 7a) [3,32]. The resulting solar cells exhibit efficiencies up to an independently certified value of 25% (V_{oc} = 723 mV, J_{sc} = 41.9 mA/cm^2, *FF* = 82.6%).

Further analysis by ILM show that our cells are limited by a lifetime degradation caused by the back-end processing. The pseudo efficiency from ILM is 26.2% before contact opening. It decreases to 26% after contact opening and to 25.7% after metallization. The decrease in implied pseudo efficiency is caused by a decrease in implied open circuit voltage from 735 mV to 728 mV and in implied pseudo-fill factor from 84.9% to 84.2%. Another factor limiting the overall efficiency is caused by recombination in the unilluminated regions around the active cell area (see [33] for a detailed analysis).

3.5. Device simulations

In order to evaluate the impact of the bulk lifetime on the cell efficiency, we perform FEM simulations of our cell structure (Fig. 7b) using Quokka [34]. Quokka uses the conductive boundary (CoBo)

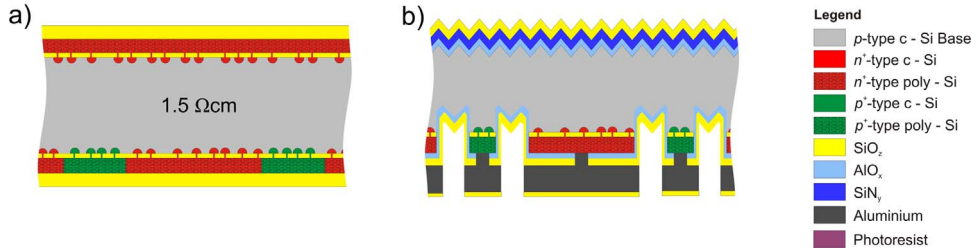

Fig. 7. a) Interim status of the cell precursor, showing the *n*-POLO junction present on the front-side for gettering purpose. b) Schematic cross section of the POLO-IBC solar cell.

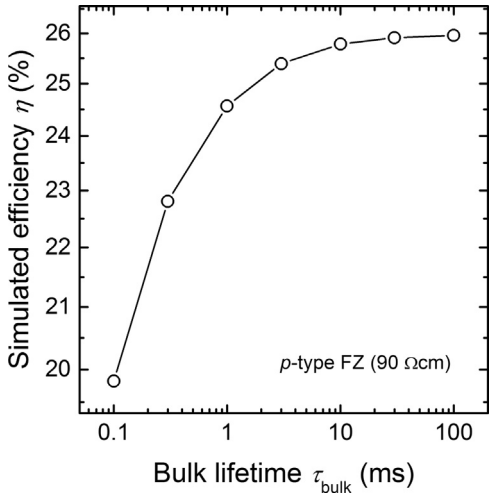

Fig. 8. Simulated cell efficiency as a function of the bulk τ_{SRH} on 90 Ωcm *p*-type FZ substrates.

model to describe the doped regions [35]. All input parameters are determined on test samples from the same cell batch, except for the contact resistances, which we set to 0.22 mΩ cm^2 for *n*-type POLO and 0.91 mΩ cm^2 for *p*-type POLO. These values are lower limit values accounting for the junction resistance between the poly-Si and the c-Si and the contact resistances between the poly-Si and the aluminum [10]. The generation profile is determined by analytical modelling of the measured hemispherical reflectance of the finished cell between 300 nm and 1200 nm thereby taking into account diffuse light scattering at both surfaces [36].

The resulting efficiencies as a function of τ_{SRH} (0.1 ms … 100 ms) are summarized in Fig. 8. For high τ_{SRH} the efficiency saturates around 26%. The difference in efficiency between 10 ms and 100 ms is only 0.2%. Nevertheless for very high efficient solar cells high quality substrates are essential [31], and an optimized POLO junction formation, especially for *n*-type POLO, can help to improve the SRH lifetime of the substrates. For a potential increase of the cell efficiency beyond 26%, further optimizations addressing the cell geometry and passivation schemes are currently under work.

4. Conclusions

We have shown that aside from their excellent recombination properties, POLO junctions offer even more benefits for the preparation of high-efficient silicon solar cells. Thus the formation *n*-type POLO junctions lead to a drastic increase of the bulk SRH lifetime in the range of 100 ms. We propose that this external gettering effect is similar to a $POCl_3$ diffusion due to the high phosphorous concentration within the poly-Si and the surface-near regions. By process of elimination we conclude Ni or another Ni-like impurity to be a likely candidate for the dominating gettered species. Our observations raises the question whether this *n*-type POLO gettering can be utilized to increase the lifetime of multicrystalline or Cz material up to a level achievable with conventional gettering techniques, e.g. conventional $POCl_3$ diffusion. Additionally we were able to implement this gettering step into a process flow of an IBC solar cell with an independently confirmed efficiency of 25%.

Acknowledgements

The authors thank Raymond Zieseniß, Guido Glowatzki Annika Raugewitz, Sabine Schmidt and Hilke Fischer for their help with the sample processing. This work was supported by the German Federal Ministry for Economic Affairs and Energy (BMWi) under contract no. 0325827C.

References

[1] M.A. Green, Corrigendum to 'solar cell efficiency tables (version 49), Prog. Photovolt.: Res. Appl. 25 (2017) 3–13.
[2] K. Yoshikawa, H. Kawasaki, W. Yoshida, T. Irie, K. Konishi, K. Nakano, T. Uto, D. Adachi, M. Kanematsu, H. Uzu, K. Yamamoto, Silicon heterojunction solar cell with interdigitated back contacts for a photoconversion efficiency over 26%, Nat. Energy 2 (2017) 17032-1–17032-8.
[3] F. Haase, F. Kiefer, J. Krügener, R. Brendel, R. Peibst, IBC solar cells with polycrystalline on oxide (POLO) passivating contacts for both polarities, Presented at the 26th International Photovoltaic Science and Engineering Conference, Singapore, 2016.
[4] U. Römer, R. Peibst, T. Ohrdes, B. Lim, J. Krügener, T. Wietler, R. Brendel, Ion implantation for poly-Si passivated back-junction back-contacted solar cells, IEEE J. Photovolt. 5 (2015) 507–514.
[5] D.E. Kane, R.M. Swanson, Measurement of the emitter saturation current by a contactless photoconductivity decay method, in: Proceedings of the 18th IEEE Photovoltaic Specialists Conference, 1985, pp. 578–583.
[6] A. Richter, S.W. Glunz, F. Werner, J. Schmidt, A. Cuevas, Improved quantitative description of Auger recombination in crystalline silicon, Phys. Rev. B 86 (2012) 165202-1–165202-14.
[7] U. Römer, R. Peibst, T. Ohrdes, B. Lim, J. Krügener, E. Bugiel, T. Wietler, R. Brendel, Recombination behavior and contact resistance of n+ and p+ poly-crystalline Si/mono-crystalline Si junctions, Sol. Energ. Mat. Sol. Cells 131 (2014) 85–91.
[8] K. Ramspeck, S. Reissenweber, J. Schmidt, K. Bothe, R. Brendel, Dynamic carrier lifetime imaging of silicon wafers using an infrared-camera-based approach, Appl. Phys. Lett. 93 (2008) 102104-01–102104-03.
[9] N.E. Grant, V.P. Markevich, J. Mullins, A.R. Peaker, F. Rougieux, D. MacDonald, J.D. Murphy, Permanent annihilation of thermally activated defects which limit the lifetime of float-zone silicon, Phys. Status Solidi A 213 (2016) 2844–2849.
[10] M. Rienäcker, M. Bossmeyer, A. Merkle, U. Römer, F. Haase, J. Krügener, R. Brendel, R. Peibst, Junction resistivity of carrier-selective polysilicon on oxide junctions and its impact on solar cell performance, IEEE J. Photovolt. 7 (2017) 11–18.
[11] S.M. Myers, M. Seibt, W. Schröter, Mechanisms of transition-metal gettering in silicon, J. Appl. Phys. 88 (2000) 3795–3819.
[12] A.A. Istratov, W. Huber, E.R. Weber, Experimental evidence for the presence of segregation and relaxation gettering of iron in polycrystalline silicon layers on silicon, Appl. Phys. Let. 85 (2004) 4472–4474.
[13] T. Isobe, H. Nakashima, K. Hashimoto, Diffusion coefficient of interstitial iron in silicon, Jpn. J. Appl. Phys. 28 (1989) 1282–1283.
[14] H. Nakashima, T. Sadoh, H. Kitagawa, K. Hashimoto, Diffusion and electrical properties of 3d transition-metal impurity series in silicon, Mat. Sci. Forum 143–147 (1994) a.594.
[15] D.A. Ramappa, W.B. Henley, Diffusion of iron in silicon dioxide, J. Electrochem. Soc. 146 (1999) 3773–3777.
[16] R. Peibst, U. Römer, K.R. Hofmann, B. Lim, T.F. Wietler, J. Krügener, N.-P. Harder, R. Brendel, A simple model describing the symmetric I-V characteristics of p polycrystalline/n monocrystalline Si, and n polycrystalline Si/p monocrystalline Si junctions, IEEE J. Photovolt. 4 (2014) 841–850.
[17] D. Tetzlaff, J. Krügener, Y. Larionova, S. Reiter, M. Turcu, R. Peibst, U. Höhne, J.-.D. Kähler, T. Wietler, TurcuEvolution of oxide disruptions: The (W)hole story about passivating contacts, in: Proceedings of the 43rdrd IEEE Photovoltaic Specialists Conference, 2016, pp. 0221–0224.
[18] A.A. Istratov, H. Hieslmair, E.R. Weber, Iron contamination in silicon technology, Appl. Phys. A 70 (2000) 489–534.
[19] J. Krügener, Y. Larionova, B. Wolpensinger, D. Tetzlaff, S. Reiter, M. Turcu, R. Peibst, J.-.D. Kähler, T. Wietler, Dopant diffusion from p+-poly-Si into c-Si, Dopant diffusion from p+-poly-Si into c-Si during thermal annealing, in: Proceedings of the 43rd IEEE Photovoltaic Specialists Conference, 2016, pp. 2451–2454.
[20] J. Schmidt, B. Lim, D. Walter, K. Bothe, S. Gatz, T. Dullweber, P.P. Altermatt, Impurity-related limitations of next-generation industrial silicon solar cells, IEEE J. Photovolt. 3 (2013) 114–118.
[21] D. MacDonald, L.J. Geerligs, Recombination activity of interstitial iron and other transition metal point defects in p- and n-type crystalline silicon, Appl. Phys. Lett. 85 (2004) 4061–4063.
[22] J.L. Benton, P.A. Stolk, D.J. Eaglesham, D.C. Jacobson, J.-Y. Cheng, J.M. Poate, N.T. Ha, T.E. Haynes, S.M. Myers, Iron gettering mechanisms in silicon, J. Appl. Phys. 80 (1996) 3275–3284.
[23] R. Hoelzl, D. Huber, K.-J. Range, L. Fabry, J. Hage, R. Wahlich, Gettering of copper and nickel in p/p+ epitaxial wafers, J. Electrochem. Soc. 147 (2000) 2704–2710.
[24] A. Ourmazd, W. Schröter, Phosphorus gettering and intrinsic gettering of nickel in silicon, Appl. Phys. Lett. 45 (1984) 781–783.
[25] M.B. Shabani, T. Yamashita, E. Morita, Study of gettering mechanisms in silicon: competetive gettering between phosphorus diffusion gettering and other gettering sites, Solid State Phenom. 131–133 (2008) 399–404.
[26] L. Baldi, G.F. Cerofolini, G. Ferla, G. Frigerio, Gold solubility in silicon and gettering by phosphorus, Phys. Stat. Sol. (a) 48 (1978) 523–532.
[27] N. Khelifati, D. Bouhafs, M. Boumaour, S.-E.-H. Abaidia, B. Palahouane, Effect of extended phosphorus diffusion gettering on chromium impurity in HEM multi-crystalline silicon, Mat. Sci. Semicon. Proc. 15 (2012) 56–60.
[28] W. Shockley, W.T. Read, Statistics of the recombinations of holes and electrons, Phys. Rev. 87 (1952) 835–842.
[29] R.N. Hall, Electron-hole recombination in germanium, Phys. Rev. 87 (1952) 387.
[30] F. Buchholz, E. Wefringhaus, S. Eisert, H. Egenolf, A. Groß, Measurement and

impact of surface transition metal contamination of textured multicrystalline silicon wafers, in: Proceedings of the 26th European Photovoltaic Solar Energy Conference, 2011, pp. 1187-1190.
[31] D.D. Smith, P. Cousins, S. Westerberg, R. De Jesus-Tabajonda, G. Aniero, Y.-C. Shen, Towards the practical limits of silicon solar cells, IEEE J. Photovolt. 4 (2014) 1465–1469.
[32] M. Rienäcker, A. Merkle, U. Römer, H. Kohlenberg, J. Krügener, R. Brendel, R. Peibst, Recombination behavior of photolithography-free back junction back contact solar cells with carrier-selective polysilicon on oxide junctions for both polarities, Energy Procedia 92 (2016) 412–418.
[33] F. Haase, F. Kiefer, S. Schäfer, C. Kruse, J. Krügener, R. Brendel, R. Peibst, IBC solar cells with polycrystalline on oxide (POLO) passivating contacts for both polarities, accepted in Jap. J. Appl. Phys, 2017.
[34] A. Fell, A free and fast three-dimensional/two-dimensional solar cell simulator featuring conductive boundary and quasi-neutrality approximations, IEEE Trans. Electron Dev. 60 (2013) 733–738.
[35] R. Brendel, Modeling solar cells with the dopant-diffused layers treated as conductive boundaries, Prog. Photo.: Res. Appl. 20 (2012) 31–43.
[36] R. Brendel, T. Dullweber, R. Peibst, C. Kranz, A. Merkle, D. Walter, Breakdown of the efficiency gap to 29% based on experimental input data and modeling, Prog. Photo.: Res. Appl. 24 (2016) 1475–1486.